

Light-induced atomic desorption and diffusion of Rb from porous alumina

S. Villalba, H. Failache, and A. Lezama

Instituto de Física, Facultad de Ingeniería, Universidad de la República, J. Herrera y Reissig 565, 11300 Montevideo, Uruguay

(Received 23 October 2009; published 15 March 2010)

We present a study of light-induced atom desorption (LIAD) of an alkali-metal atom (Rb) in porous alumina. We observe the variation due to LIAD of the rubidium density in a vapor cell as a function of illumination time, intensity, and wavelength. The simple and regular structure of the alumina pores allows a description of the atomic diffusion in the porous medium in which the diffusion constant only depends on the known pore geometry and the atomic sticking time to the pore wall. A simple one-dimensional theoretical model is presented which reproduces the essential features of the observed signals. Fitting of the model to the experimental data gives access to the diffusion constant and consequently the atom-wall sticking time and its dependence on light intensity and wavelength. The nonmonotonic dependence of the LIAD yield on the illumination light frequency is indicative of the existence of Rb clusters in the porous medium.

DOI: [10.1103/PhysRevA.81.032901](https://doi.org/10.1103/PhysRevA.81.032901)

PACS number(s): 79.20.Ds, 68.43.Tj, 66.30.Pa, 47.61.-k

I. INTRODUCTION

In a spectroscopic cell containing an alkali-metal-atom vapor, a substantial fraction of the atoms are adsorbed on the cell walls. At steady state, the gas density is in equilibrium with the adsorbed fraction of atoms. In some cells, depending on the cell material or coating, when the cell is illuminated with moderate-intensity ($1\text{--}1000\text{ mW/cm}^2$) nonresonant light, a significant increase in the atomic vapor density is produced as a consequence of the release of atoms from the cell surface into the gas phase. Such effect has been named light-induced atomic desorption (LIAD) [1].

LIAD has received considerable attention in recent years due to its application as a light-controlled atom dispenser under high vacuum conditions. Such dispenser has been successfully used to load magneto-optical atom traps [2–4] and hollow optical fibers [5–7]. Its use has also been considered for atomic magnetometers, gyroscopes, and clocks [8,9]. In addition, LIAD has attracted the attention of astrophysicists since it has been related to the observed abundance of alkaline elements in nonpermanent extraterrestrial atmospheres [10].

LIAD was first observed in sodium-vapor glass cells in which the inner cell walls were coated with a thin layer of polydimethylsiloxane (PDMS). The effect was observed with K [11], Rb, and Cs atoms [12]. Initially, it was considered that LIAD was specific to PDMS coatings [13]. However, LIAD was later reported in cells coated with different polymers such as octadimethyl-cyclotetrasiloxane (OCT) [14] and paraffin [12]. More recently, LIAD has been studied in porous amorphous materials such as porous silica [15]. LIAD has also been observed on some uncoated surfaces, such as glass [4,7], stainless steel [4], and sapphire [16].

LIAD is understood as a nonthermal effect, as opposed to light desorption produced with high-power sources in which a significant heating results from light absorption by the substrate. In PDMS [13] and paraffin [12] a frequency threshold in the infrared, similar to that of the photoelectric effect on metals, has been observed. Also, an increasing efficiency of LIAD with light frequency has been reported [12,17,18].

All observations of LIAD in porous or coated surfaces present some common features, such as the characteristic time scale of the atomic desorption (several seconds). However, other aspects may vary significantly between different atomic species and coatings depending also in the cell preparation procedure. In particular, large variations are observed in the desorption yield. In cells coated with PDMS, LIAD may result in an increase of the atomic gas-phase density of several orders of magnitude [13] while density-increase factors of only a few units were reported for paraffin [12]. Smaller factors were observed on the present study. The question on whether there is a common mechanism underlying LIAD observations in different physical systems is still open [19].

The first tentative explanation of LIAD at the microscopic level was suggested by Xu *et al.* [13]. The mechanism involves the modification by light of the weakly bonded chemical complex formed between a PDMS molecule and the Na atom or Na_2 molecule. More recently, this mechanism was further investigated through the measurement of the thermal distribution of desorbed atom velocities [20]. This interpretation of LIAD is consistent with the observation of a threshold light frequency for LIAD in PDMS but leaves unexplained several aspects of its dynamics. As discussed by Atutov *et al.* [17], in addition to the atomic desorption from the surface, the diffusion of the atoms within the surface coating plays an essential role in the temporal evolution of LIAD. To a large extent, LIAD in coated surfaces is a consequence of light-induced modification of the atomic mobility and diffusion within the coating polymer. Atutov *et al.* [17] have modeled such a process assuming a phenomenological dependence of the diffusion coefficient on light. Alexandrov *et al.* have described the LIAD dynamics with the help of rate equations with a light-dependent term representing the flux of atoms from the coating into the gas phase [12]. Recently, the model of LIAD in coated surfaces suggested by Atutov has been revised and improved by Rebilas and co-workers [21,22].

A precise modeling of LIAD should involve the simultaneous account of the successive occurrence of two distinctive processes: (i) atomic desorption from the surface and (ii) diffusion in the intermediate medium (either the polymer or the porous medium) prior to the atom release in the

vapor phase. The desorption mechanism is at present only qualitatively understood [13,20,23]. Also, little understanding is currently available on the mechanisms determining the variation with light of the atomic mobility in the polymer coating. Diffusion in porous silica is presumably simpler since the atomic motion inside the pores may be assumed to occur in a diluted vapor. However, the random nature of the pore geometry complicates the modeling of such process.

An additional difficulty for the LIAD description in porous materials comes from the fact that alkaline atoms can be either individually adsorbed on the material surface or agglomerated into clusters. The presence of clusters may result in a visible change of the sample transparency or even in coloration [24]. Blue-green coloration by Rb of otherwise transparent (or white) samples has been observed in several experiments, including the ones described here. The role of the light in these samples is double since it can produce the direct desorption of the atoms from the dielectric surface and the evaporation of the atomic clusters [23,25]. Also, under suitable conditions, the light may also control the growth of the clusters from atoms in the vapor phase. Such conditions are favored in porous media where the desorbed atoms remain confined and available to participate in the cluster regrowth. A characteristic feature of the LIAD involving cluster evaporation, is the nonmonotonic dependence of the desorption yield on the light frequency. Such behavior is interpreted as the consequence of resonant surface plasmon excitation in the cluster [23]. A second characteristic of these systems is its “memory.” The response strongly depends on the illumination history including the timing of the bright and dark periods and the corresponding color sequence [23].

We present an experimental study of LIAD with Rb atoms adsorbed in thin membranes of porous alumina. The porous alumina is obtained by anodization of aluminum and results in a very regular array of cylindrical pores with small size dispersion. In this work, we take advantage of the accurate knowledge of the porous medium geometry to study LIAD under particularly simple conditions in which the diffusion process of the atoms inside the pores, as well as the release of atoms from the porous medium into the cell volume, are determined by the pore geometry through simple kinetic theory considerations with no need for additional phenomenological transport parameters. We model the diffusion process as the result of a random sequence of free flight of the atoms confined within the pore wall. After a collision with the wall, the atom sticks to the wall for some time, after which it is desorbed again, flying with random direction and velocity. Eventually, diffusing atoms may reach the pore end and are released into the cell volume. Our observation of the atomic density variation in the cell due to LIAD allows us to determine the atomic diffusion constant inside the pores. In turn, the knowledge of the diffusion constant gives access to the atom-wall sticking time and its dependence on light intensity and color.

The article is organized as follows. In Sec. II we describe the experimental setup. The experimental observations are presented in Sec. III. In Sec. IV we describe the theoretical model and the fitting of the experimental data that allow the measurement of diffusion constant and the mean sticking time of atoms to the pores surfaces. Conclusions are presented in Sec. V.

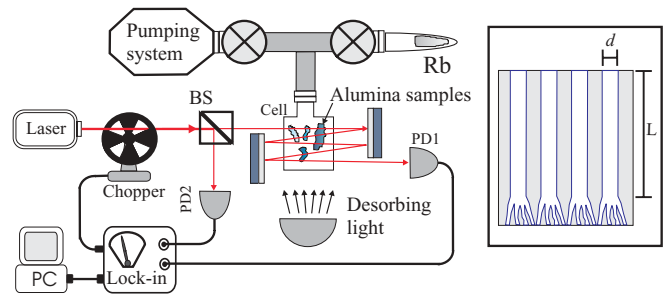


FIG. 1. (Color online) Experimental setup. (Inset) Schematic cross section of the alumina membrane for a plane parallel to the pores. BS, beam splitter; PD1, PD2, photodetectors.

II. EXPERIMENT

We have used porous alumina membranes manufactured by Whatman International Limited. The circular flat membranes have a diameter of 1 in. and a thickness of $60 \mu\text{m}$. The membrane is traversed by a regular array of hollow cylindrical tubes with 200 nm diameter. The tubes form a honeycomblike array with a pore density of $10^9/\text{cm}^2$. The diameter of the pores are uniform over most of their length. On one side of the membrane, along $1 \mu\text{m}$, the pores divide into several smaller branches with 20 nm typical diameter (see the inset in Fig. 1). Before contact with the Rb vapor the porous membranes are translucent and white. In order to fit into the vacuum glass cell, the membranes are divided into pieces of typically 0.5 cm^2 .

The experimental setup is shown in Fig. 1. We have used a $2.5 \times 2.5 \times 4.5\text{-cm}$ glass vacuum cell. The cell is connected via a glass-to-metal transition fitting to an ion pump and a metallic Rb reservoir. The Rb density in the glass cell is monitored by measuring the absorption of a laser beam issued from an extended-cavity diode laser. Using a saturated absorption setup, the laser frequency is stabilized to the ^{85}Rb $F = 3 \rightarrow F' = 4$ transition in the D_2 line (780 nm). In order to increase the absorption signal, the laser beam crosses the cell several times. We have used a balanced detection scheme to reduce sensitivity to laser intensity fluctuations. Half of the laser power is sampled before the cell and detected with a photodiode. A second photodiode monitors the intensity of the beam transmitted through the cell. The outputs of the two photodiodes are subtracted. In order to eliminate noise from ambient light, including the light used for the LIAD, the laser beam is modulated with a chopper and lock-in detected. The illumination of the porous alumina samples is effected with high-power light-emitting diodes (LEDs) (100 mW) in order to have a nonthermal source with a well-defined spectrum. Three different LEDs were used centered at 455 , 504 , and 617 nm (typical spectral width 10 nm). An optical arrangement (not shown in Fig. 1) allows a uniform illumination of the porous sample by the LED light.

Prior to the introduction of the porous alumina membrane, the glass cell was evacuated (10^{-6} torr) and baked for several hours at 300°C . Such a precaution appeared to be essential since we have observed significant LIAD from the unbaked cell, presumably due to some uncontrolled coating. After the baking procedure, the LIAD from the cell walls was negligible. Following the cell cleanup, several pieces of the alumina membrane were introduced and vacuum baked for several days

at 150°C. The pieces of alumina lay on the cell bottom. We had no control on the side of the membrane that faces the cell wall, so some of the pieces present the largest pore apertures toward the cell bulk volume while others present the narrow ramification ends. After the initial cleanup of the alumina, the cell was returned to room temperature and the valve separating the cell from the metallic Rb reservoir opened. Keeping the Rb reservoir and the vacuum connecting tubes slightly heated ($\sim 50^\circ\text{C}$), the Rb was allowed to diffuse into the cell and the porous alumina. After a few days, a visible blue coloration appeared in the alumina, indicating the presence of Rb. After a sufficiently long period all the samples were dark blue. However, two different blue tones were observed among the samples. We interpret such difference as a consequence of the two possible orientations of the membrane pieces with respect to the cell wall. The blue coloration is an indication of the formation of Rb clusters [24]. We have checked that the cluster formation is entirely reversible. The original white coloration of the alumina could be recovered after pumping the cell during a few hours while illuminating with an incandescent lamp.

III. EXPERIMENTAL RESULTS

We have observed the LIAD of Rb from the porous alumina by monitoring the laser absorption in the cell bulk while turning on and off the illumination by a LED. We have recorded the relative variation of the vapor density $\delta(t) \equiv [\rho(t) - \rho_0]/\rho_0$ as a function of time, where $\rho(t)$ is the density of Rb in the cell and ρ_0 the equilibrium density in the dark. Figure 2 shows two typical records obtained with the same illumination for two different light-on intervals (500 and 600 s). In general, the relative density reaches a maximum δ_{\max} after a few tens of seconds depending on light intensity. After that, the Rb density slowly decreases toward a new steady state in the presence of light. When the light is turned off, δ decreases on a time scale comparable to the rise time. Two different behaviors have been observed for long times after the light switching off. Either the density returns monotonically to the initial equilibrium density ρ_0 or drops below ρ_0 by an amount ε (see Fig. 2), after which it slowly grows toward ρ_0 . The latter behavior is observed if the light intensity and the illumination interval are sufficiently large.

Figure 3 shows the evolution of the Rb density in the cell for two different illumination intensities. Notice the variation in the shapes of the traces. Similar shape variations were also observed in experiments with porous silica [15], although not reproduced by the proposed theoretical models.

We have observed that the efficiency of the LIAD process depends on the porous alumina history, as was also noticed in other systems [12,23]. A monotonic reduction in the maximum relative Rb density variation δ_{\max} is observed for several successive illumination cycles, keeping constant the light intensity. In addition, as the intensity is changed between successive illumination periods, the signal variation is different depending on whether the light intensity is increased or decreased (see Fig. 4). For low-enough light intensities the system is not appreciably modified by the illumination and a linear dependence of the LIAD yield on light intensity is observed. The nonlinear dependence, visible in Fig. 4 for large

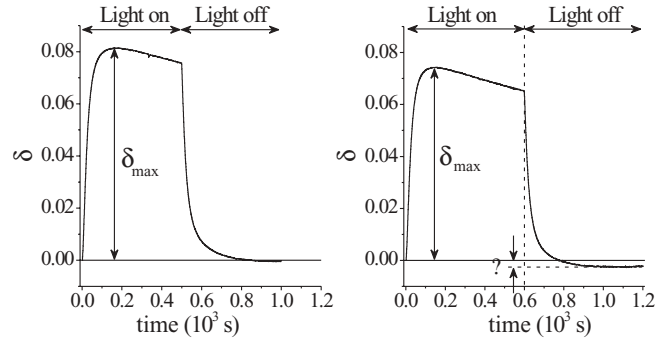


FIG. 2. Typical observed variations of the relative atomic vapor density for two different illumination-time intervals. Illumination: $I = 50 \text{ mW/cm}^2$; $\lambda = 617 \text{ nm}$.

intensities, can be attributed to the depletion of the available Rb inside the nanopores.

Figure 5 shows δ_{\max} as a function of illumination intensity for three different wavelengths. The measurements were taken alternating the three available light colors successively for each intensity. The effect of the history on the LIAD efficiency is so reduced for the comparison among measurements taken with different wavelengths. In Fig. 5 the nonlinear variation of δ_{\max} is only noticeable for the highest intensities.

From the linear fit of the data in Fig. 5 one can evaluate, for each wavelength, the coefficient $\alpha_\lambda \equiv \delta_{\max} \hbar \omega / I$ proportional to the LIAD desorption rate per photon flux. We observe that this coefficient for blue, green, and red light varies in proportion to 1, 0.73, and 1.1, respectively. Such result indicates a nonmonotonic evolution of the LIAD yield with photon energy.

IV. THEORETICAL MODEL

We model the evolution of the atomic density inside the cylindrical pores as a one-dimensional diffusion process. The typical sticking time τ_s of alkali-metal atoms on dielectric surfaces is of the order of tens to hundreds of microseconds. After desorption, the atoms leave the internal surface of

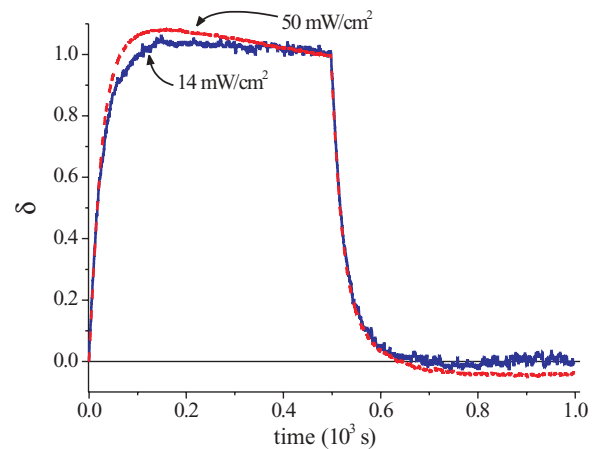


FIG. 3. (Color online) Two records of the relative atomic density variation illustrating the difference in shape for different illumination intensities (blue light). The traces have been rescaled to illustrate the differences in shape.

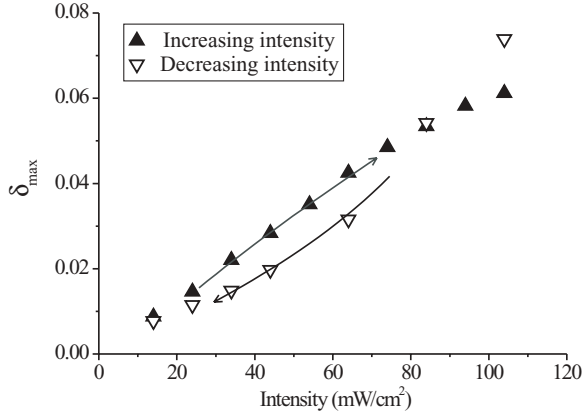


FIG. 4. Maximum relative atomic density δ_{\max} as a function of the illumination intensity (blue light). The measurements were registered with a sequence of illumination intervals of 140 s followed by intervals of 600 s without illumination. Solid (hollow) triangles, increasing (decreasing) illumination intensity.

the pore with thermal velocity in a random direction with a Lambertian probability distribution [26]. The gas density inside the pores is considered sufficiently low to neglect the collisions between flying atoms. At room temperature and for tube diameters of the order of a few hundreds of nanometers, after a few nanoseconds flight, the atom is again adsorbed on the pore surface. Since the pore length is much larger than its diameter, we can consider that the atoms execute a one-dimensional random walk along the pore axis, characterized by the diffusion constant (see Appendix),

$$D = \frac{\langle l^2 \rangle}{2\tau} = \frac{d^2}{3\tau}, \quad (1)$$

where $\langle l^2 \rangle$ is the mean square displacement per step in the random walk, τ is the mean interval between steps, which is essentially determined by the sticking time $\tau \simeq \tau_s$ on the internal pore surface, and d is the pore diameter.

The atomic desorption is described by a reduction of τ_s induced by the light. We assume a simple linear dependence,

$$\tau_s = \tau_{s0}(1 - \kappa I), \quad (2)$$

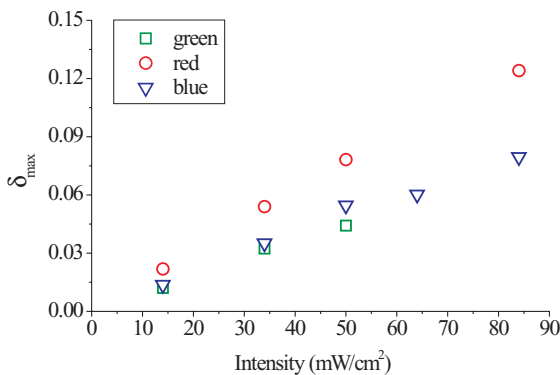


FIG. 5. (Color online) Maximum relative atomic density δ_{\max} as a function of the illumination intensity for different illumination wavelengths (455, 505, and 617 nm). Illumination time interval, 500 s.

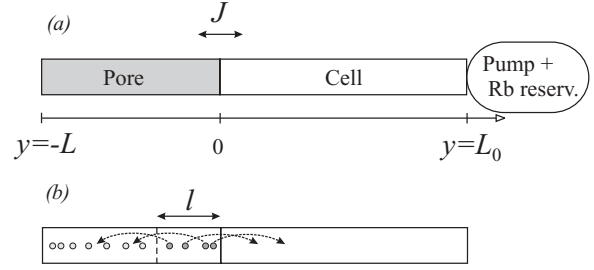


FIG. 6. (a) Schematic one-dimensional model for the system. (b) Illustration of the atomic release from the pore end into the gas cell [J^+ in Eq. (8)].

where τ_{s0} is the sticking time in the dark, I is the light intensity, and κ a coefficient which is wavelength dependent. In consequence,

$$D = \frac{D_0}{(1 - \kappa I)}, \quad (3)$$

with $D_0 = d^2/(3\tau_{s0})$ being the atomic diffusion constant in the dark.

Figure 6 presents a scheme of the one-dimensional model of the system. The cylindrical pore, considered closed on its left end, has a total length L . To the right of the pore, the atomic vapor cell, associated to a length L_0 , is connected to a reservoir accounting for the vacuum pumping and the external Rb reservoir.

The (linear) density of atoms $\mu(y, t)$ inside the pore is described by the diffusion equation

$$\frac{\partial \mu}{\partial t} = D \frac{\partial^2 \mu}{\partial y^2}, \quad (4)$$

where y is the position coordinate inside the pore (see Fig. 6).

The total number of atoms N in the cell is $N = N_g + N_w$, where N_g represents the atoms in the gas phase and N_w the atoms adsorbed to the cell walls. The fraction of atoms in the gas phase relative to the total number of atoms is assumed to be a constant for given temperature and illumination conditions [27]:

$$\frac{N_g}{N} = \frac{L_0}{L_0 + \Delta}. \quad (5)$$

Here Δ represents an effective cell length corresponding to adsorbed atoms. Since the sticking time of the atoms to the cell walls can, in principle, depend on light intensity, we consider that Δ depends on the illumination in the form $\Delta = \Delta_0(1 - \zeta I)$, where ζ is a coefficient that can depend on wavelength. The evolution of the atom number N in the cell is described by the equation

$$\frac{dN}{dt} = \frac{dN_g}{dt} \left\{ 1 + \frac{\Delta}{L_0} \right\} = J - \gamma(N_g - N_{g0}), \quad (6)$$

where J is the net atomic flux at the pore-vapor interface. The rate γ describes the return to the equilibrium atom number N_{g0} determined by the external pumping system and Rb reservoir.

We separate the net flux J into two contributions, $J = J^+ + J^-$, describing the atoms leaving and entering the pore, respectively. The flux of atoms entering the pores from the cell

gas is given by

$$J^- = -\frac{\bar{v}}{2L_0}N_g, \quad (7)$$

where $\bar{v} \equiv \langle |v_y| \rangle$ is the mean magnitude of the atomic velocity in the direction of the pore. The simple geometry of our system allows the evaluation of J^+ without additional assumptions by considering that the atoms within a mean step length l from the pore end have a probability of 1/2 for leaving the pore in the time interval τ [see Fig. 6(b)]; then

$$J^+ = [\mu(0)l] \frac{1}{2} \frac{1}{\tau} \simeq \mu(0) \frac{D}{l}, \quad (8)$$

where we have made the approximation $l \simeq \langle l^2 \rangle^{\frac{1}{2}}$.

The equations describing the evolution of the atomic densities μ and $n \equiv N_g/L_0$ inside the pores and in the cell gas phase, respectively, are

$$\frac{\partial \mu}{\partial t} = D \frac{\partial^2 \mu}{\partial y^2}, \quad (9a)$$

$$\frac{dn}{dt} = \frac{D}{lL_c(1-\sigma I)}\mu(0) - \frac{\left(\tilde{\gamma} + \frac{\bar{v}}{2L_c}\right)}{(1-\sigma I)}n + \frac{\tilde{\gamma}}{(1-\sigma I)}n_0, \quad (9b)$$

where we have introduced the parameters $\sigma \equiv \frac{\zeta}{(1+\frac{L_0}{\Delta_0})}$, $L_c \equiv (L_0 + \Delta_0)$ and $\tilde{\gamma} \equiv \frac{\gamma L_0}{L_c}$. n_0 is the equilibrium value of the atomic density in the vapor cell.

The steady-state densities in the dark inside the pores μ_0 and in the vapor cell n_0 are linked through the condition

$$J = \frac{D_0}{l}\mu_0 - \frac{\bar{v}}{2}n_0 = 0. \quad (10)$$

The boundary conditions at the pore ends are [see Eqs. (7) and (8)]

$$-D \frac{\partial \mu}{\partial y} \Big|_{y=0} = \frac{D}{l}\mu(0) - \frac{\bar{v}}{2}n, \quad (11a)$$

$$\frac{\partial \mu}{\partial y} \Big|_{y=-L} = 0. \quad (11b)$$

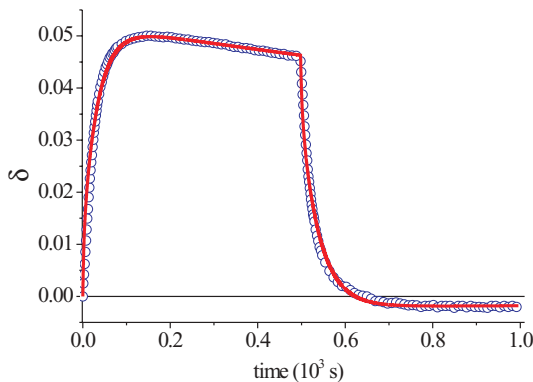


FIG. 7. (Color online) Example of the fitting of the calculated signal (solid line) to the experimental data (circles). Blue light, $I = 50 \text{ mW/cm}^2$.

From the preceding equations, it is possible to derive an approximate relation between the observed variation of the gas density in the cell and the corresponding change in the diffusion constant inside the pores. For this we notice that in our system, the return to equilibrium (under constant illumination) occurs on time scale which is long compared to the observation time. One can then consider that during the LIAD the total atomic population (inside the pores and in the cell) remains approximately constant,

$$\int_0^L \mu(y)dy + n(L_0 + \Delta) \simeq \left(\frac{l\bar{v}}{2D_0}L + L_c \right) n_0, \quad (12)$$

where we used Eq. (10).

When the sample is illuminated, the LIAD effect redistributes the atoms along the pore in a characteristic diffusion time $L^2/2D$. If we assume that the gas-phase density reaches its maximum n_{\max} in a time which is of the order or longer than the diffusion time, one can consider that the corresponding atomic density inside the pores is approximately uniform $\mu \simeq \mu_{\max}$. Within this approximation, Eqs. (6) (with $\gamma = 0$) and (12) give

$$J = \frac{D}{l}\mu_{\max} - \frac{\bar{v}}{2}n_{\max} = 0, \quad (13)$$

$$\mu_{\max}L + n_{\max}L_c \simeq \left(\frac{l\bar{v}}{2D_0}L + L_c \right) n_0, \quad (14)$$

where we have neglected the contribution of atoms desorbed by the light from the cell walls ($\Delta \approx \Delta_0$). Using Eqs. (13) and (14), we obtain

$$\delta_{\max} \approx \frac{n_{\max} - n_0}{n_0} = \frac{(D - D_0)}{D_0} \frac{1}{\left(1 + \frac{2DL_c}{\bar{v}lL}\right)}. \quad (15)$$

Equation (15) can be used for a quick estimate of the relative variation of the diffusion constant from the observed change in the vapor density, provided the second term inside the brackets in Eq. (15) is small. In the conditions of our experiment, such a term is of the order of unity.

Some of the parameters appearing in the model can be directly determined for our system. From the porous alumina manufacturer we know that $L = 60 \text{ } \mu\text{m}$ and $d = 200 \text{ nm}$. Therefore, $\langle l^2 \rangle = \frac{2}{3}d^2 \approx 1.6 \times 10^{-7} \text{ m}^2$. The mean atomic velocity at room temperature is $\bar{v} \approx 140 \text{ m/s}$. The other parameters are determined through least-square fitting of the numerical model to the experimental data. For this, we have numerically integrated the differential Eqs. (9) with the boundary conditions given in Eqs. (11).

Figure 7 shows a typical experimental register together with the corresponding signal calculated from the model. The values of the parameters obtained from the fitting are presented in Table I. The given uncertainties correspond to the scattering of the results of the fitting for different experimental runs. The value of D_0 given in Table I results from the average of the data obtained with all three excitation wavelengths. Interestingly enough, the plot of the fitted values of D_0 for different runs reveals a systematic grouping for each of the three colors used for LIAD (see Fig. 8). In our model, D_0 , corresponding to the diffusion constant in the dark, is taken as constant and independent of the desorbing light color. However, the

TABLE I. Fitted values of the parameters of the model.

D_0 ($\text{m}^2 \text{s}^{-1}$)	L_0 (m)	γ (s^{-1})	σ [$(\text{mW}/\text{cm}^2)^{-1}$]	κ_{red} [$(\text{mW}/\text{cm}^2)^{-1}$]	κ_{green} [$(\text{mW}/\text{cm}^2)^{-1}$]	κ_{blue} [$(\text{mW}/\text{cm}^2)^{-1}$]
$2.8 \pm 0.5 \times 10^{-11}$	106 ± 33	$2.4 \pm 1.5 \times 10^{-4}$	$2.2 \pm 2.0 \times 10^{-3}$	$7.8 \pm 0.7 \times 10^{-3}$	$4.6 \pm 0.5 \times 10^{-3}$	$5.2 \pm 0.5 \times 10^{-3}$

grouping observed in Fig. 8 may reveal a dependence of D_0 on the illumination history. Such a feature could be an indication of cluster formation and cluster-light interaction. The investigation of cluster formation is outside the scope of this work.

We notice that the value of L_0 in Table I is large compared to the length ($\lesssim 10$ m) estimated from the actual glass cell volume. However, the total effective volume available to the atoms outside the porous alumina also depends on the vacuum system tubes and surfaces [8]. Distinct values of the coefficient κ are obtained depending on the wavelength of the illuminating light. The parameter σ reflects a dependence of the effective cell length on the illumination. The need for such a parameter in our model can be questioned starting from the initial observation of no LIAD in the clean, empty cell prior to the introduction of the alumina samples. However, after the introduction of the alumina and after several weeks during which the glass cell was connected to the pumping system and rubidium reservoir, we cannot exclude the possibility of LIAD from an uncontrolled glass surface coating or the alumina surface between pores. The numerical fitting is quite insensitive to this parameter, giving a large scattering of the results. Such uncertainty prevents the determination of a wavelength dependence of this parameter. Nevertheless, a nonzero value of σ was used in the numerical calculation for a better adjustment of the shape of the observed variation of the rubidium density as a function of time.

From the parameters in Table I we can check that the assumptions made for the derivation of Eq. (15) are reasonable for our system. The estimate of the maximum relative vapor density variation obtained using Eq. (15) only differs in a few percents from the value resulting from the numerical integration of Eqs. (9).

A comparison of the predictions of the theoretical model with the experimental observations is given in Fig. 9 for traces

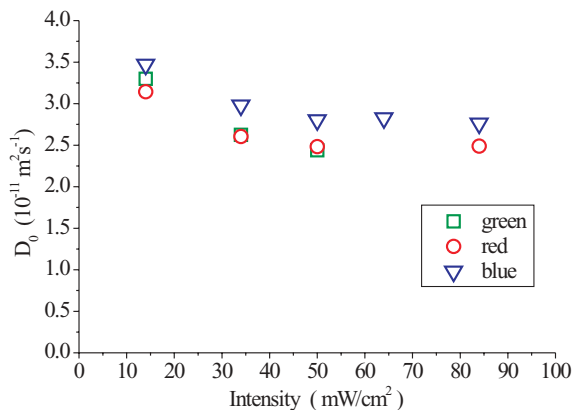


FIG. 8. (Color online) Values of the diffusion constant D_0 obtained from the fitting of different experimental traces obtained with three illumination colors. Illumination interval, 600 s.

obtained with blue desorbing light. Except for the largest intensities, where the effects of saturation and illumination history are expected to be significant, the model correctly describes the growth of the LIAD signal with light intensity. Similar results are obtained for the other colors used for illumination.

Our theoretical model appears to account for several features of the experimental signal. As shown in Fig. 10, the signal shape variation as a function of the illumination time interval is well described. In particular, the “undershoot” ε of the vapor density below the initial density is well reproduced. Such undershoot is due to the small variation of the total number of atoms (due to the external pumping system) during illumination. As the illumination is turned off, the atoms are rapidly readsorbed by the porous alumina in a time shorter than that required to equilibrate the cell with the external pump and Rb supply. Our model is not able to reproduce the details of the temporal-evolution shape when the illumination intensity is varied. Such details are better appreciated in Fig. 11, where the traces calculated for two different intensities are normalized. Comparison of these traces with those in Fig. 3 show that

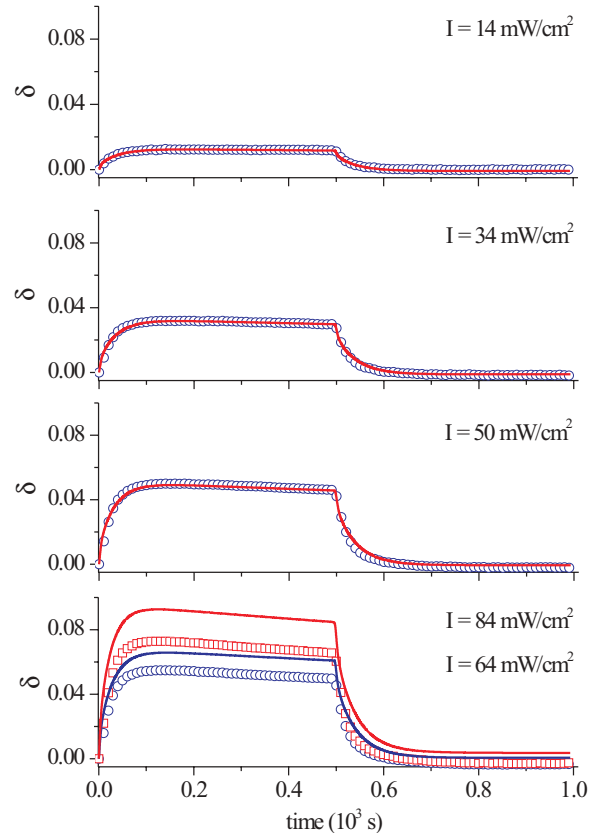


FIG. 9. (Color online) Comparison of the experimental data (circles and squares) with the calculated signal (solid lines) obtained with the parameters in Table I for $\lambda = 455$ nm.

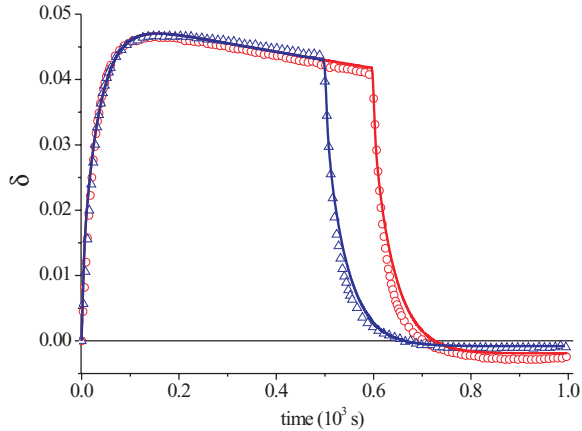


FIG. 10. (Color online) Observed (circles and triangles) and calculated (solid lines) signals for two illumination intervals. Blue light, $I = 50$ mW.

our model cannot simultaneously reproduce in detail the rise and decrease of the signal. This discrepancy may be due to unaccounted-for processes such as those depending on sample history.

From the measured value of D_0 using Eq. (1), one can determine the sticking time τ_s of the atoms to the pore walls. The obtained value $\tau_{s,0} \simeq 500 \mu\text{s}$ lies within the range of previous observations for alkali-metal atoms on dielectric surfaces. A summary of the sticking times reported in the literature for several alkali-metal atoms and surfaces is presented in Table II. The value of τ_s is several orders of magnitude larger than the mean time of flight of the atoms between collisions with the pore walls $\tau_0 \sim 1$ ns. At a given time, the fraction of atoms in the gas phase inside the pores relative to the total number of atoms participating in the diffusion is $\tau_0/\tau_s \sim 10^{-5}$. From the values in Table I, we estimate a relative variation of the atomic gas density within the pores of 60% for illumination with $50 \text{ mW}/\text{cm}^2$ of red light.

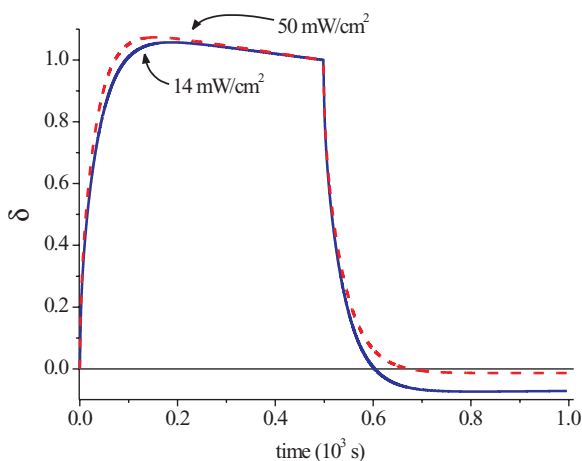


FIG. 11. (Color online) Calculated traces for different (blue light) illumination intensities. The plots have been rescaled to illustrate the differences in shape.

TABLE II. Reported alkali-metal-atom-dielectric surface sticking times at room temperature.

Atom and surface	Sticking time (μs)	Comments
Cs and Pyrex	1400	[27]
Cs and sapphire	<160	[27]
Na and glass	130	[28]
Rb and alumina	500	This work

V. CONCLUSIONS

We have studied LIAD of Rb atoms contained within alumina nanopores. We observed, as a function of time, the variations of the Rb density in the cell surrounding the porous alumina as illuminating light of different colors is turned on and off. We have shown that the observed signal evolution is determined by the diffusive motion of Rb atoms within the porous medium. Our observations are consistent with the picture of atoms undergoing a one-dimensional random walk along the porous axis. Taking advantage of the well-characterized geometry of the porous medium, a simple relation of the diffusion coefficient with the pore diameter and the atom-wall sticking time was established. Also, at the pores ends, the atom exchange between the gas cell and the porous medium is directly linked, without additional assumptions, to the parameters of the diffusive motion [Eq. (8)].

The measurement of the diffusion constant gives direct access to the mean time between steps. This time is essentially a sticking time as the atoms remain most of the time absorbed to the pore wall. Our results indicate a linear decrease of the sticking time with the illuminating light intensity for low light intensity. In addition, the sticking time modification appears to be dependent on the illuminating light frequency. The LIAD yield does not vary monotonically with light frequency for the three wavelengths used. This suggests that the atom release takes place, at least in part, from rubidium clusters where surface plasmon resonances contribute to the light-absorption spectrum [23,24].

ACKNOWLEDGMENTS

The authors acknowledge support from ANII (Fondo Clemente Estable), CSIC, and ECOS-Sud.

APPENDIX: CALCULATION OF THE DIFFUSION COEFFICIENT IN A CYLINDRICAL PORE

For a one-dimension random walk in the direction y , assuming that the length and duration of the random steps are uncorrelated, the diffusion constant is given by [29]

$$D = \frac{\langle l_y^2 \rangle}{2\tau} = \frac{\langle v_y^2 t^2 \rangle}{2\tau}, \quad (\text{A1})$$

where l_y is the single step displacement in the direction y , v_y is the y component of the particle velocity, and t the time of flight of a given step. τ is the mean time interval between steps.

We consider particles free flying within the inner surface of cylinder with diameter d . A particle leaving the cylinder wall

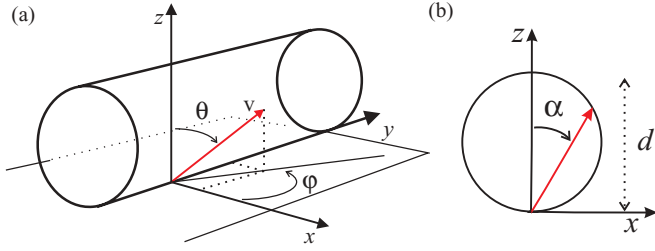


FIG. 12. (Color online) (a) Cylinder and coordinate system considered in the calculation. (b) Cross-section along the x - z plane.

has a velocity given by

$$\begin{aligned} v_z &= v \cos(\theta), \\ v_y &= v \sin(\theta) \sin(\phi), \\ v_x &= v \sin(\theta) \cos(\phi), \end{aligned} \quad (\text{A2})$$

where v is the velocity modulus. See Fig. 12 for angle definitions.

The time of flight is given by

$$t = \frac{l_{x,z}}{v_{x,z}}, \quad (\text{A3})$$

where $l_{x,z}$ and $v_{x,z}$ are the projections of the particle displacement and velocity over the x - z plane. We have

$$l_{x,z} = d \cos(\alpha) = d \frac{v_z}{v_{x,z}}. \quad (\text{A4})$$

Using Eqs. (A2), (A3), and (A4), we obtain

$$t = \frac{d \cos(\theta)}{v [\cos^2(\theta) + \sin^2(\theta) \cos^2(\phi)]} \quad (\text{A5})$$

and

$$l_y = v_y t = \frac{d \sin(\theta) \cos(\theta) \sin(\phi)}{[\cos^2(\theta) + \sin^2(\theta) \cos^2(\phi)]}. \quad (\text{A6})$$

The angular (Lambertian) distribution of the atoms leaving the surface is given by [26]

$$P(\Omega) d\Omega = \cos(\theta) d\Omega, \quad (\text{A7})$$

where Ω is the solid angle. The thermal distribution for the magnitude of the atomic velocity is [26]

$$P(v) = \frac{1}{2} \left(\frac{m}{k_B T} \right)^2 v^3 \exp\left(-\frac{v^2}{v_{\text{rms}}^2}\right), \quad (\text{A8})$$

with $v_{\text{rms}} = \sqrt{\frac{2k_B T}{m}}$.

Using (A6) and (A7), after integration one gets

$$\langle l_y^2 \rangle = \frac{2}{3} d^2. \quad (\text{A9})$$

In a similar way, from (A5), (A7), and (A8), we obtain

$$\tau_0 = \langle t \rangle = d \sqrt{\frac{2\pi m}{k_B T}}. \quad (\text{A10})$$

In our system, the time interval between flights is determined by the atom sticking time τ_s ($\tau \simeq \tau_s \gg \tau_0$).

-
- [1] A. Gozzini, F. Mango, J. H. Xu, G. Alzetta, F. Maccarrone, and R. A. Bernheim, *Nuovo Cimento* **15**, 709 (1993).
- [2] B. P. Anderson and M. A. Kasevich, *Phys. Rev. A* **63**, 023404 (2001).
- [3] S. N. Atutov *et al.*, *Phys. Rev. A* **67**, 053401 (2003).
- [4] C. Klempt, T. van Zoest, T. Henninger, O. Topic, E. Rasel, W. Ertmer, and J. Arlt, *Phys. Rev. A* **73**, 013410 (2006).
- [5] S. Ghosh, A. R. Bhagwat, C. K. Renshaw, S. Goh, A. L. Gaeta, and B. J. Kirby, *Phys. Rev. Lett.* **97**, 023603 (2006).
- [6] P. Londero, V. Venkataraman, A. R. Bhagwat, A. D. Slepikov, and A. L. Gaeta, *Phys. Rev. Lett.* **103**, 043602 (2009).
- [7] A. R. Bhagwat, A. D. Slepikov, V. Venkataraman, P. Londero, and A. L. Gaeta, *Phys. Rev. A* **79**, 063809 (2009).
- [8] T. Karaulanov *et al.*, *Phys. Rev. A* **79**, 012902 (2009).
- [9] A. Bogi, C. Marinelli, A. Burchianti, E. Mariotti, L. Moi, S. Gozzini, L. Marmugi, and A. Lucchesini, *Opt. Lett.* **34**, 2643 (2009).
- [10] B. V. Yakishinskiy and T. E. Madey, *Surf. Sci.* **528**, 54 (2003).
- [11] S. Gozzini and A. Lucchesini, *Eur. Phys. J. D* **28**, 157 (2004).
- [12] E. B. Alexandrov, M. V. Balabas, D. Budker, D. English, D. F. Kimball, C.-H. Li, and V. V. Yashchuk, *Phys. Rev. A* **66**, 042903 (2002).
- [13] J. H. Xu, A. Gozzini, F. Mango, G. Alzetta, and R. A. Bernheim, *Phys. Rev. A* **54**, 3146 (1996).
- [14] J. H. Xu, Ph.D. thesis, Scuola Normal Superiore, 1994.
- [15] A. Burchianti *et al.*, *Europhys. Lett.* **67**, 983 (2004).
- [16] A. M. Bonch-Bruевич, Y. N. Maksimov, S. G. Przhibelskii, and V. V. Khormov, *Sov. Phys. JETP* **65**, 161 (1987).
- [17] S. N. Atutov, V. Biancalana, P. Bicchi, C. Marinelli, E. Mariotti, M. Meucci, A. Nagel, K. A. Nasyrov, S. Rachini, and L. Moi, *Phys. Rev. A* **60**, 4693 (1999).
- [18] E. Mariotti, M. Meucci, C. Marinelli, P. Bicci, and L. Moi, in *Proceedings of the XII International Conference on Laser Spectroscopy* (World Scientific, New York, 1996), p. 390.
- [19] R. J. Hamers, *Surf. Sci.* **583**, 1 (2005).
- [20] J. Brewer, V. G. Bordo, M. J. Kaspruwicz, and H. G. Rubahn, *Phys. Rev. A* **69**, 062902 (2004).
- [21] K. Rebilas and M. J. Kaspruwicz, *Phys. Rev. A* **79**, 042903 (2009).
- [22] K. Rebilas, *Phys. Rev. A* **80**, 014901 (2009).
- [23] A. Burchianti, A. Bogi, C. Marinelli, C. Maibohm, E. Mariotti, and L. Moi, *Phys. Rev. Lett.* **97**, 157404 (2006).
- [24] A. Burchianti, A. Bogi, C. Marinelli, E. Mariotti, and L. Moi, *Opt. Express* **16**, 1377 (2008).
- [25] A. Burchianti, A. Bogi, C. Marinelli, C. Maibohm, E. Mariotti, S. Sanguinetti, and L. Moi, *Eur. Phys. J. D* **49**, 201 (2009).
- [26] F. O. Goodman and H. Y. Wachman, *Dynamics of Gas-Surface Scattering* (Academic Press, San Diego, 1976).
- [27] M. Stephens, R. Rhodes, and C. Wieman, *J. Appl. Phys.* **76**, 3479 (1994).
- [28] V. G. Bordo and H. G. Rubahn, *Opt. Express* **4**(2), 59 (1999).
- [29] E. Ott, *Chaos in Dynamical Systems* (Cambridge University Press, Cambridge, UK, 1993).